Impact of molecular rearrangement of amphiphilic stabilizers on physical stability of itraconazole nanoparticles prepared by flash nanoprecipitation

Ka Yee Wan[1], Ka Wai Wong[2], Albert Hee Lum Chow[1,*], Shing Fung Chow[3,*]

[1]School of Pharmacy, The Chinese University of Hong Kong, Sha Tin, Hong Kong

[2]HL Science & Technology Limited, Kowloon, Hong Kong

[3]Department of Pharmacology and Pharmacy, The University of Hong Kong, Pokfulam, Hong Kong

* *Corresponding authors*

Albert H. L. Chow
School of Pharmacy,
The Chinese University of Hong Kong,
8/F, Lo Kwee-Seong Integrated
Biomedical Sciences Building, Area 39,
Shatin, N.T., Hong Kong
Email: albert-chow@cuhk.edu.hk
Tel: 852 26096829
Fax: 852 26035295

Shing Fung Chow
Department of Pharmacology and Pharmacy
Li Ka Shing Faculty of Medicine
The University of Hong Kong
L2-08B, Laboratory Block,
21 Sassoon Road, Pokfulam, Hong Kong
Email: asfchow@hku.hk
Tel: 852 39179026
Fax: 852 28170859

Abbreviations

AFM	Atomic force microscopy
AS	Amphiphilic stabilizer
FNP	Flash Nanoprecipitation
ITZ	Itraconazole
MIVM	Multi-inlet vortex mixer
PEG-PLA	Poly(ethylene glycol)-b-poly(DL-lactide)
PI	Polydispersity index
$R_{D:H+L}$	Relative ratio of ITZ to the total hydrophilic and hydrophobic parts of the stabilizer
$R_{H:D+L}$	Relative ratio of hydrophilic part of the stabilizer to ITZ plus hydrophobic part of the stabilizer
$R_{H:L}$	Relative ratio of hydrophilic to hydrophobic part of stabilizers
TPGS	d-α-tocopheryl polyethylene glycol 1000 succinate
XPS	X-ray photoelectron spectroscopy
δ	Solubility parameter

ABSTRACT: Flash nanoprecipitation (FNP) is a controlled antisolvent precipitation process that has proven effective for consistent production of drug nanoparticles with a defined mean particle size and narrow particle size distribution. However, physical instability of the generated nanoparticles remains a major challenge in the application of this technology in pharmaceutical formulation. Aimed at resolving this problem, the present study has investigated the FNP process and associated stabilization mechanism of itraconazole (ITZ) nanoparticles through in-depth nanoparticle characterization. Results showed that ITZ nanoparticles could be reproducibly produced with a mean particle size < 100 nm and a polydispersity index < 0.2 in the presence of amphiphilic stabilizers (ASs). Surface analysis of freshly formed nanoparticles by X-ray photoelectron spectroscopy (XPS) revealed initially a disordered packing structure and subsequently a time-dependent molecular rearrangement of incorporated AS towards a micelle-like structure. The faster the molecular rearrangement of AS, the more stable the nanoparticles, as monitored by the change in particle size with time. These findings may have important implications for the selection of effective ASs for formulating stable drug nanoparticles. The present study is the first of its kind to demonstrate the utility of XPS to track the molecular transport of stabilizers in rapidly generated nanoparticles.

Keywords: itraconazole; flash nanoprecipitation; nanoparticle stability; amphiphilic stabilizers; molecular reorientation; surface analysis; X-ray photoelectron spectroscopy

1. Introduction

The application of solid nanoparticles in drug delivery has been an active area of pharmaceutical research for decades. As a drug delivery system, they offer a good number of unique advantages. For instance, their extremely large surface area to volume ratio accounts for their significantly higher saturation solubility and dissolution rate compared to their coarse counterparts. This unique characteristic has been successfully exploited in the solubility enhancement of poorly water-soluble drugs (Zhang et al., 2017). Specifically, drug-loaded polymeric nanoparticles with particle size below 200 nm have been shown capable of crossing biological barriers (Fernandes et al., 2010), mitigating first-pass hepatic metabolism (Italia et al., 2007) and displaying enhanced permeability and retention (EPR) effect (Allen and Cullis, 2004).

Nano-sized solid particles for drug delivery encompass polymeric micelles, polymer-stabilized nanoparticles, solid lipid nanoparticles, and nanocrystals. Among these nanoparticulate drug delivery systems, polymer-stabilized nanoparticles and polymeric micelles have been most extensively investigated owing to their ease of preparation and their readily modifiable surface properties to achieve desired delivery outcomes, e.g., specific site targeting. Polymer-stabilized nanoparticles are commonly prepared by antisolvent precipitation which is perhaps the simplest and most cost-efficient method for generating ultrafine particles within a short time-scale (Chan and Kwok, 2011). The technique strictly applies to hydrophobic solutes, and requires the use of an amphiphilic stabilizer (AS), commonly a diblock copolymer. The stabilizer protects the hydrophobic solute by forming a micelle or micelle-like structure with its hydrophilic groups protruding into external aqueous media (to maintain particle dispersion) and its hydrophobic groups holding the hydrophobic solute within the particle core via hydrophobic interaction. In addition, the surface hydrophilicity of the nanoparticles can greatly reduce their in vivo opsonization and subsequent clearance by the reticuloendothelial system. To achieve active targeting, the hydrophilic moiety of the polymer can be chemically modified by attachment of a site-specific ligand (Nasongkla et al., 2006). Despite these advantages, the antisolvent precipitation process is difficult to control and the resulting nanoparticles tend to be

physically unstable.

As a means of tackling the process controllability issue, flash nanoprecipitation (FNP), a controlled antisolvent process, has been subsequently developed (Johnson and Prud'homme, 2003). Process control is mainly achieved by using a specially designed mixer such as confined impinging jet (CIJ) mixer and multi-inlet vortex mixer (MIVM) (Chow et al., 2014; Liu et al., 2008a), which provide high-efficiency mixing of all components present. Employing various amphiphilic co-block polymers as stabilizers, the technology has proven effective for consistent production of nanoparticles with a defined mean particle size (< 200nm) and a narrow particle size range (Chow et al., 2015; Zhu et al., 2007). However, in spite of its high efficiency and excellent reproducibility, FNP has been successfully applied to the production of stable nanoparticles for only a limited number of highly hydrophobic compounds or drugs including beta-carotene (Zhu et al., 2010), paclitaxel (Saad, 2007) and bifenthrin (Liu et al., 2008b). To ensure good nanoparticle stability, it has been suggested that the compound involved must have a log P value of over 6 (Zhang et al., 2017; Zhu, 2014). However, drugs typically have log P values between 3 and 6, which inevitably raise serious instability issue when they are prepared as nanoparticles by FNP.

The instability problem with nanoparticles of less lipophilic drugs has been further investigated by Zhu, who attributed this problem to the non-equilibrium packing arrangement (i.e., non-micellar structure) of the ASs in the nanoparticles when they first emerged from solutions (Zhu, 2013). The author suggested that the hydrophilic PEG segments of the ASs were partly embedded inside the particle core, leading to partial exposure of the hydrophobic segments to the external aqueous medium. In contrast, Pustulka et al. showed that the PEG segment of the stabilizer, PEG-PLGA, was situated on the nanoparticle surface and proposed a three-layer nanoparticle structure consisting successively of a drug core, a shell of PLGA and a corona of PEG (Pustulka et al., 2013). The controversy over the actual packing structures of ASs in various nanoparticle preparations is perhaps not unexpected, as most of the reported studies appeared to have overlooked the time-dependent molecular rearrangement of ASs in the nanoparticles subsequent to their formation.

Owing to their non-equilibrium state when the AS-encased nanoparticles first appear from solution, the AS molecules in the nanoparticles will undergo rearrangement in the nanoparticles with time until attaining a micelle-like or the most stable structure, especially for those ASs of low molecular weights, which tend to show a high molecular mobility. The faster the molecular rearrangement of AS in nanoparticles, the sooner the attainment of the most stable or micelle-like structure and the more stable the nanoparticles in the suspending media. Thus, the kinetics of molecular rearrangement of ASs appears to play an important role in determining the stability and shelf-life of final nanoparticle products. To probe into this issue further, the present study has employed itraconazole (ITZ) as a model drug to prepare nanoparticles with different ASs by FNP for subsequent stability testing.

Itraconazole [log P = 5.66 (Miyama et al., 1998)] is an antifungal drug with a broad spectrum of activity, but only used as second- or third-line antifungal mainly because of its low and erratic oral bioavailability. This is closely associated with its extremely low aqueous solubility (~1ng/ml) (Jung et al., 1999) and extensive first-pass metabolism (Van Peer et al., 1989). It can be envisaged that formulating ITZ into nanoparticles not only can augment its aqueous solubility, but can also improve its *in vivo* delivery. Rabinow and co-workers showed that the apparent plasma half-life of ITZ nanosuspensions with a mean particle size of ~580 nm was much larger than that of ITZ solution formulation (~15.6 h as opposed to ~5.05 h) after intravenous administration, reflecting the sustained action of ITZ nanosuspensions (Rabinow et al., 2007). Thus far, extremely few of the reported ITZ nanoparticle formulations with particle size below 200 nm have been evaluated *in vivo* for pharmacokinetic properties and biodistribution. It was found that the plasma concentration of ITZ nanoparticles with particle size of ~200 nm was prolonged at a defined concentration (Kim et al., 2010) and that the distributions of ITZ nanoparticles of ~110 nm in the lungs, liver and spleen were enhanced after intravenous administration (Chen et al., 2008). However, the therapeutic utility of ITZ nanoparticles at the low end of this particle size range is conceivably very limited due to the increasing deteriorating stability of ITZ nanoparticles when their size approaches the true nano-size range (< 100 nm). In fact, ITZ-loaded nanoparticles

with particle size less than 200 nm have never been reported to be stable at room temperature. Kumar and co-workers described their nanosuspension as being the finest (~145 nm) yet stable preparation, but the apparently good stability in terms of particle size was only observed after the nanosuspension was dialyzed to remove the organic solvent present and stored at 5ºC (Kumar et al., 2009). The nanoparticles still grew to a size of ~758 nm (~4.2 fold increase) after a storage period of 3 h at room temperature.

Thus, in the present work, we hypothesize that the stabilizer in the nanoparticles formed initially remains in a disordered and dynamic state, and undergoes molecular rearrangement towards the most stable state (i.e., micelle-like structure with hydrophilic groups on the particle surface and hydrophobic groups in the particle core) in a time-dependent manner, and that this rearrangement process has an important bearing on the nanoparticle stability. Accordingly, the main objectives of the present study were threefold: (a) to prepare ITZ nanoparticles smaller than 100 nm by FNP with different ASs; (b) to monitor the storage stability of the ITZ-AS nanoparticles in terms of the change in particle size with time; and (c) to examine the time-dependent change in surface composition of freshly formed ITZ-AS nanoparticles by XPS and AFM.

2. Materials and methods

2.1. Materials

ITZ (Purity > 99%) was purchased from Yick-Vic Chemicals & Pharmaceuticals Ltd. (Hong Kong, China). Poly(ethylene glycol)-b-poly(DL-lactide) (PEG-PLA) of different molecular weights (MW~2k-2k; 2k-10k; 5k-10k) and d-α-tocopheryl polyethylene glycol 1000 succinate (TPGS) were obtained from SRI Biomaterials Inc. (California, USA) and Sigma Aldrich (USA) respectively. Analytical grade dimethylformamide (DMF) and tetrahydrofuran (THF) were supplied by RCI Labscan Ltd and Merck KGaA. Ammonium acetate was purchased from Sigma Aldrich (USA). HPLC grade acetonitrile (ACN) was supplied by Duksan Pure Chemicals (Kyungkido, Korea), and analytical grade acetic acid was obtained from BDH Laboratory Supplies (UK). Water used was deionized with a final

resistivity not less than 18.0 MΩ·cm by a water purification system (Direct-QTM, Millipore, USA).

2.2. Preparation of ITZ nanoparticles

ITZ nanosuspensions were produced by FNP using a four-stream MIVM. The experimental set-up of MIVM is depicted in Fig. 1. In brief, one stream of the mixer contained an organic solvent (DMF) while the other three streams consisted of water serving as antisolvent. ITZ and AS at equal mass concentration (i.e., 5mg/ml) were dissolved in the organic solvent. Rapid mixing of the organic and aqueous phases in the mixer was precisely controlled at defined flowrates by means of two digital programmable syringe pumps (PHD 2000, Harvard apparatus, MA, USA). The organic stream (inlet A) and one of the aqueous streams (inlet C) were set at the same flowrate while the remaining two aqueous streams (inlets B and D) formed another flow equivalent pair. The flowrates of inlets B and D were set at 9 times higher than those of inlets A and C in order to create a sufficiently high supersaturation of drug for rapid precipitation. In the present study, Reynold number was kept at 4,139 whose corresponding mixing rate was found to be sufficient for achieving homogeneous mixing of all stream components prior to nanoprecipitation, as based on our previous findings (Chow et al., 2014). The resulting nanosuspension containing a final concentration of 5% v/v residual organic solvent was collected at the outlet stream of the MIVM.

2.3. Particle size analysis

Intensity-weighted particle size distribution of nanosuspensions was determined without dilution or filtration in a glass cuvette using a Delsa™ Nano C analyzer (Beckman Coulter, Inc., USA) equipped with a dual 30mW laser (with λ = 658nm). The analyzer utilizes dynamic light scattering (DLS), which measures the fluctuation in time of laser light intensity scattered by the particles in a fluid, with a scattering angle of 165^{o}. Based on the application of single-exponential fitting, cumulants analysis, and CONTIN particle size distribution analysis of the received signals, intensity-weighted particle size and size distribution (polydispersity index, PI)

were calculated. The nanosuspensions would be regarded as unstable and their stability study would be terminated if coarse particles became visible or if the DLS-measured particle size was larger than 1 μm.

2.4. High performance liquid chromatography (HPLC)

ITZ was assayed by HPLC using a Waters 2695 system equipped with a photodiode array detector (PDA), and a C18 column (symmetry®, 5μm, 4.6mm × 150mm, Waters Corporation, USA). The mobile phase, composed of ACN/10mM ammonium acetate solution adjusted to ~pH 5.7 by acetic acid (60:40 v/v), was eluted isocratically at 1 ml/min. Ten microliters of sample was injected and the detection wavelength was set at 261 nm. The retention time of ITZ was ~10 min.

2.5. Drug encapsulation efficiency determination

Drug encapsulation efficiency was calculated as the amount of drug entrapped in nanoparticles divided by the total amount of drug in the sample. Amount of drug entrapped in nanoparticles was determined by subtracting the amount of free drug from the total amount of drug in the sample. The amount of drug in the filtrate (i.e., the amount of free drug) after centrifugation of 0.5ml of the nanosuspension in an Amicon® Ultra-0.5 30K centrifugal filter device (Millipore Corp., Billerica, MA, USA) at 14000 × g for 15 min (ultrafiltration) was measured by HPLC. The filter membrane is made of low-binding regenerated cellulose. Drug concentration of the nanosuspension (i.e., total amount of drug in the sample) was also determined by HPLC.

2.6. Drug mass percentage determination

Ultrafiltration was conducted by centrifuging 15 ml of the nanosuspension in an Amicon® Ultra-15 30K centrifugal filter device (Millipore Corp., Billerica, MA, USA) at 4000 × g for 20 min. The same type of filter membrane was used as before. The residue of the nanosuspension after ultrafiltration and the nanosuspension without ultrafiltration were freeze-dried. Each freeze-dried product was weighed and then dissolved in THF for assay of drug content by HPLC. Drug loading (i.e., drug mass

percentage of the nanosuspension with ultrafiltration) was calculated as the amount of drug in the nanoparticles (i.e., drug content in the product processed by ultrafiltration) divided by the total mass of nanoparticles (weight of the product processed by ultrafiltration). Drug mass percentage of the nanosuspension without ultrafiltration is the ratio of drug content in the product to weight of the product without ultrafiltration treatment. If the extent of dissociation of AS from the particle surface is high and the concentration of free drug is negligible, drug mass percentage of the nanosuspension without ultrafiltration will be smaller than drug loading.

2.7. Zeta potential analysis

Zeta potential of nanoparticles was measured using the same equipment as that for measuring the particle size and size distribution, i.e., Delsa™ Nano C analyzer, which analyzes electrical voltage converted from electrophoretic mobility. Positive surface charge is commonly deduced from positive zeta potential and vice versa.

2.8. Determination of glass transition temperatures of PEG-PLAs

Glass transition temperature (T_g) of each PEG-PLA of defined MW was measured using a differential scanning calorimeter (DSC 6000, Perkin Elmer Corp., USA). An accurately weighed sample (2-5mg) was placed in a sealed aluminum pan. To eliminate its thermal history, each sample was heated to temperatures above its melting point at a heating rate of 10°C/min under nitrogen purge (20 ml/min) and then rapidly cooled to -60ºC. T_g of the sample was determined in the second cycle of heating to 60ºC at a heating rate of 10ºC/min.

2.9. Surface composition analysis

Samples were analyzed by X-ray photoelectron spectroscopy (XPS), which is a standard technique for determining the surface elemental composition of a particle at a depth of 5-10nm (Bascom and Chen, 1991). XPS spectra of raw materials, blank and drug-loaded nanoparticles were recorded using a Kratos Axis Ultra DLD multi-technique surface analysis system (Shimadu, Japan) with a monochromatized Al

K-α X-ray (hv 1486.6eV) source. Samples of raw materials and blank nanoparticles for XPS were prepared by the following methods: (i) recrystallization from acetone and (ii) FNP using an MIVM under the same processing conditions as the preparation method of drug-loaded nanoparticles. Samples right after production and after storage of 2 h were placed on silica wafers and air-dried overnight. Survey scans (binding energy, BE = 0-1400eV), narrow scans of C1s (BE = 274-299eV) and N1s (BE = 390-410eV) envelopes were conducted for the wafers with pass energy of 40eV. The angle of X-ray was 90°. Deconvolution of C1s peaks was performed using XPSPeak (version 4.1) software. The deconvoluted peaks were assigned to their corresponding carbon species based on the spectral data in the Handbook of X-ray and Ultraviolet Photoelectron Spectroscopy (Briggs, 1977) and the National Institute of Standards and Technology (NIST) XPS Database (Version 4.1; http://srdata.nist.gov/xps). Possible charging effects on the samples were minimized by aligning BE of all peaks with reference control by adjusting BE of C-C/C-H peak to 285.0eV. The relative compositions of different components were then calculated based on the areas under the peaks.

2.10. Analysis of surface morphology and phase imaging

Atomic force microscopy (AFM) was employed to examine the surface morphology and for phase imaging analysis of nanoparticles. Samples were mounted on glass wafers, air dried and scanned by a Tapping Mode™ atomic force microscope (TM-AFM, Dimension 3100, Digital Instruments, USA) with rotated silicon probes of tip radius less than 10 nm, spring constant of 40 N/m (range: 20-75N/m) and resonance frequency of 300 kHz (±100 kHz). Cantilever length was fixed at 125 μm (±10 μm). A set-point ratio (spr; ratio of engaged oscillation amplitude to free air oscillation amplitude) of 0.6-0.9 was employed for all AFM images.

2.11. Statistical analysis

All material testing and measurements were conducted in triplicate with separate batches of samples, and the collected data were analyzed statically by unpaired Student’s t-test at the 5% level of significance.

3. Results and discussion

3.1. Initial particle size and stability of ITZ nanoparticles

Being relatively non-toxic and having a relatively low clearance rate in the body, PEGs have been widely employed as stabilizers in pharmaceutical formulations. PEGylated excipients such as TPGS and PEG-PLA with amphiphilic character can readily adsorb on hydrophobic drug nanoparticles and serve as effective stabilizers for such nanomaterials. Both TPGS and PEG-PLA are approved by the U.S. Food and Drug Administration (FDA) for use as excipients in pharmaceutical preparations. In addition, TPGS has been reported to be capable of enhancing bioavailability and cytotoxicity of anti-cancer drugs through inhibition of P-glycoprotein and circumvention of multi-drug resistance (Cholkar et al., 2014; Collnot et al., 2006; Collnot et al., 2007). PEG-PLAs of different molecular weights are commercially available for evaluating the influence of molecular size of AS on the formation of ITZ nanoparticles. Thus, the present study has assessed these excipients for potential protection of the ITZ nanoparticles.

Fig. 2 shows the initial particle size of ITZ nanoparticles prepared with TPGS and PEG-PLA. The data indicated that ITZ nanosuspensions with initial particle size below 200 nm could be readily and reproducibly generated by FNP using the MIVM. Incorporation of TPGS produced the smallest ITZ nanoparticles (i.e., size = 91.1 nm ± 5.9 nm and PI = 0.101 $\pm$ 0.031, which is within the true nanoscale).

Fig. 3 displays the stability profiles of ITZ nanosuspensions using TPGS and PEG-PLA stored at room temperature and sub-ambient storage temperature (4°C). All the nanoparticle formulations showed improved physical stability at 4°C. Similar finding was reported by Kumar et al for PS-b-PEO-coated ITZ nanoparticles (~145 nm) which remained stable when stored at 5°C but not at ambient temperature (Kumar et al., 2009). Although particle aggregation and particle growth cannot be entirely suppressed after nanoparticle production, the short-term stability of the formulated nanoparticles, as determined by the increase in particle size of nanoparticles after 2 h of storage at room temperature (~80 nm for the most stable formulation in the present study), is significantly better than the other reported cases

of storage stability for particular ITZ nanoparticle formulations in the literature.

Improvement of particle stability at sub-ambient storage temperature can be achieved through a reduction in Ostwald ripening, desorption rate of ASs and in particle collision. The rate of Ostwald ripening, which depends on the solute concentration in solution, can be reduced by lowering the temperature. Any AS capable of solubilizing drug or enhancing drug solubility in water will promote Ostwald ripening, and a decrease in temperature will reduce drug solubility (if dissolution is endothermic) and the tendency and rate of Ostwald ripening. Since TPGS is soluble in water but PEG-PLA is not, TPGS should be more able to solubilize ITZ in water. Hence TPGS-stabilized ITZ nanoparticles would be less prone to Ostwald ripening when stored at refrigerated temperature due to a reduced concentration of free drug. To verify if this was the case, the concentration of free drug in freshly prepared ITZ-TPGS nanosuspensions was determined by HPLC. Drug loading of the formulation (49.9% ± 0.55%) was found to accord with the theoretical value (50%), and drug encapsulation efficiency was nearly 100% (> 99%) with negligible amount of free drug (< 2.834×10^{-3}mM) being detected in the suspending medium, indicative of essentially complete encapsulation of ITZ. Liu et al. studied quantitatively the Ostwald ripening of β-carotene nanosuspension produced by FNP (Liu et al., 2007). In their study, by decreasing THF to water ratio in the precipitation medium, they demonstrated a reduction in both β-carotene solubility and Ostwald ripening. Ostwald ripening appeared insignificant (i.e., particle size only increased by not more than 10 nm over 15 days) when β-carotene solubility was at 0.04 mM, which was much higher than the ITZ concentration used in the preparation of ITZ-TPGS nanosuspensions. This finding further substantiates the utility of storage at sub-ambient conditions for enhancing ITZ nanoparticle stability by minimizing Ostwald ripening.

Since the potential contribution of Ostwald ripening to the instability of ITZ nanoparticles had been ruled out, the other possible cause for instability would be particle aggregation. Among the ASs being tested, TPGS is the most water-soluble stabilizer and should exhibit the highest desorption rate from ITZ nanoparticles. As with free drug, desorbed TPGS can also be separated from ITZ nanoparticles and

removed from suspending medium by ultrafiltration. The proportion of TPGS desorbed can be estimated from the mass percentages of drug in freeze-dried products obtained from ITZ-TPGS nanosuspensions with and without ultrafiltration. Assuming that the mass of free drug is negligible, an increase in the mass percentage of drug after ultrafiltration will be a result of TPGS desorption from ITZ nanoparticles. No significant difference in drug mass percentage was found for freeze-dried nanosuspensions with and without ultrafiltration (49.9% ± 0.55% without ultrafiltration; 50.1% ± 1.56% with ultrafiltration; $p > 0.05$), indicative of negligible TPGS desorption.

Temperature can also influence the collision rate of nanoparticles in aqueous media. The viscosity of suspending medium, as well as the diffusivity and kinetic energy of nanoparticles will decrease when the storage temperature is lowered from ~20°C (ambient) to 4°C (sub-ambient). This will reduce the particle collision frequency and hence the chance of particle aggregation.

3.2. Stabilization mechanisms of ASs

Typical stabilization mechanisms of stabilizers for colloidal suspensions via surface adsorption are steric hindrance and ionic stabilization. ITZ nanosuspensions are stabilized by ASs whose hydrophilic moieties reside on the particle surface to form a steric barrier against particle aggregation and particle growth. The extent of steric hindrance depends on the size or bulkiness of the hydrophilic groups in the ASs. On the other hand, ionic stabilization relies on the ionization of ASs to generate charged groups on the particle surface, which prevent particle aggregation by electrostatic repulsion. The extent of ionization of ASs will determine the strength of electrostatic repulsion. In the present study, the involvement of surface charges in the stabilization mechanism was investigated by zeta potential measurements, and the data were analyzed for potential correlation with initial particle size and storage stability (Fig. 4). Since ITZ itself showed negligible ionization in the aqueous suspending medium, as confirmed by the low zeta potential (-5.45mV ± 0.95mV) of its stabilizer-free nanoparticles, any significant change in the measured zeta potential is likely to be mainly contributed by the stabilizer on the particle surface. ASs

afforded low zeta potentials in magnitude (<10 mV in magnitude), which accord with the relatively low ionization of TPGS and PEG-PLA.

Zeta potential was found to have no apparent correlation with the initial particle size and stability of ITZ nanoparticles. The lack of surface charge effect on initial particle size can be explained by the fact that particle growth from nuclei is governed by adsorption of ASs on the growing nuclei through hydrophobic interaction but not ionic interaction. On the other hand, nanoparticle stability is determined by the ionization of ASs to form charged groups on particle surface for preventing particle aggregation by electrostatic repulsion. In general, only surface charges of sufficient magnitude (corresponding to zeta potential greater than +30mV or less than -30mV) are considered effective for stabilizing nanosuspensions by electrostatic repulsion (Jacobs et al., 2000). ITZ nanoparticles are thus mainly protected by steric hindrance of ASs.

3.3. Effect of size and composition of ASs

To quench further particle growth and prevent particle aggregation, ASs need to diffuse and adsorb rapidly on the ITZ nuclei during particle formation. If the time of arresting nucleus growth is sufficiently long, ASs will self-orientate towards their most stable equilibrium molecular arrangement (i.e., all hydrophobic tails adsorbing on the hydrophobic ITZ core and all hydrophilic heads protruding into the surrounding water) since they are employed at concentrations above their critical micelle concentrations (CMCs) (Table 1). Nevertheless, considering the highly efficient mixing and extremely rapid particle formation in FNP (Russ et al., 2010), it is speculated that the orientation of co-precipitating AS is initially not at the most stable equilibrium state right after nanoparticle formation. The growth arresting times with different ASs on nanoparticles should be very short and thus the differences in diffusivities of the ASs would not have any critical impact on nanoparticle formation. Based on consideration of the growth arresting time alone, the ITZ nanoparticles with different ASs should have similar initial particle sizes. Nevertheless, the actual situation is far more complicated. From Fig. 2, it can be seen that the initial particle sizes of the samples varied with ASs, implying that AS can affect particle growth not

only by surface adsorption, but also by other, possibly more important, mechanisms.

To focus on the influence of molecular size of AS on the formation of ITZ nanoparticles, three PEG-PLAs (2k-2k; 2k-10k; 5k-10k) were employed in the study. It was found that the initial particle size of nanoparticles was larger with a longer hydrophobic PLA block (PEG-PLA: 2k-2k versus 2k-10k; $p < 0.05$) (Fig. 2). This finding is consistent with the results reported by Riley et al. which revealed an increase in the particle size of blank PEG-PLA nanoparticles with an increase in the length of PLA block (Riley et al., 2001). Since the size distribution of ITZ nanoparticles with PEG-PLA was unimodel, the amount of blank PEG-PLA nanoparticles could be assumed to be negligible in the system. This suggests that PEG-PLA co-precipitated with ITZ and interfered with its subsequent growth. The hydrophobic envelope constructed by PLA limits the amount of ITZ encapsulated. Longer PLA block is expected to provide a larger capacity for accommodating the hydrophobic drug in the core and thereby give rise to larger initial particle size. On the other hand, the initial particle size of nanoparticles was smaller with a longer hydrophilic PEG block (PEG-PLA: 2k-10k versus 5k-10k; $p < 0.05$) (Fig. 2). The space occupied by PEG on the surface of nanoparticles is different with different lengths of PEG, resulting in a different packing structure of PEG-PLA. This has been supported by the observation that while diblock copolymers of large volume fraction of hydrophilic PEG/PEO ($f_{EO} > 0.50$) generated relatively small spherical aggregates, that of small f_{EO} (0.2-0.42) formed vesicles with relatively thick corona structure (Ahmed and Discher, 2004).

Since ASs attach to ITZ mainly through hydrophobic interaction, larger hydrophobic segments of ASs should possess higher hydrophobicity and adsorb more tightly on particle surface. On the other hand, larger hydrophilic segments of ASs should provide stronger steric hindrance. Thus ASs comprised of longer hydrophilic and hydrophobic blocks should produce much more stable nanoparticles. However, this inference appears to be in discordance with the results in Fig. 5, which show that TPGS with relative small mass for both hydrophilic and hydrophobic segments yielded the most stable ITZ nanosuspension. This is perhaps not surprising as TPGS has a different chemical structure which can influence the resulting strength of

hydrophobic interaction and steric hindrance. In addition, the effect of structure-dependent re-orientation of ASs on particle stability should not be discounted.

For the three PEG-PLAs of different PEG and/or PLA block lengths, but of the same basic structural PEG and PLA units, the stability of ITZ nanoparticles increased with an increase in PEG block length (PEG-PLA: 2k-10k versus 5k-10k; $p < 0.05$) (Fig. 3). This can be attributed to greater steric hindrance provided by the longer PEG block. However, the stability of the nanoparticles was shown to decrease with an increase in PLA block length (PEG-PLA: 2k-2k versus 2k-10k; $p < 0.05$) (Fig. 3), which appears to contradict the general belief that longer PLA block should exhibit stronger adsorption on the hydrophobic particle core and hence yield more stable nanoparticles. All these observations suggest that the molecular re-orientation of PEG-PLA in nanoparticles is unlikely to be directionally specific.

3.4. Surface composition of ITZ-AS nanoparticles

As discussed before, the formation of ITZ-AS nanoparticles by FNP may be so rapid that the AS molecules have no sufficient time to self-assemble into the most stable configuration or micelle-like structure under equilibrium conditions, i.e., with all hydrophobic segments residing in the hydrophobic core and all hydrophilic segments protruding into the surrounding water. To verify if this was indeed the case, elemental composition of the particle surface of the nanoparticles was analyzed by XPS. After deconvolution, all the peaks in C1s envelop can be grouped into three categories: (i) $C_{(285)}$ (BE = 285.0eV), (ii) $C_{(286\text{-}288)}$ (BE = 286 - 288eV) and (iii) $C_{(288\text{-}290)}$ (BE = 288 - 290eV), as depicted in Fig. 6. While $C_{(285)}$ and $C_{(288\text{-}290)}$ are contributed by ITZ ($C_{(285),ITZ}$ and $C_{(288\text{-}290),ITZ}$) and hydrophobic (lipophilic) part of AS ($C_{(285),L,AS}$ and $C_{(288\text{-}290),L,AS}$), $C_{(286\text{-}288)}$ is borne by all segments including ITZ ($C_{(286\text{-}288),ITZ}$), hydrophilic part of AS ($C_{(286\text{-}288),H,AS}$) and hydrophobic (lipophilic) part of AS ($C_{(286\text{-}288),L,AS}$). Typical deconvolution of C peaks is shown in Fig. 7. It should be noted that the signal of Cl was too weak for analysis due to its relatively small atomic composition in ITZ. Since TPGS and PEG-PLA do not contain any nitrogen (N) atom in their chemical structures, nitrogen atom in ITZ molecules (N_{ITZ}) can

serve as a “tracer” both qualitatively and quantitatively for the presence of ITZ on the surface of ITZ-TPGS and ITZ-PEG-PLA nanoparticles. All theoretical values were calculated based on the assumption of uniform distribution and an absence of preferred orientation of all interested chemical species in the nanoparticles.

With regards to the systems containing pure materials only (i.e., ITZ, TPGS or PEG-PLA), it was found that the atomic concentration ratios of N_{ITZ}:$C_{(286\text{-}288),ITZ}$:$C_{(288\text{-}290),ITZ}$ on pure ITZ particle surface analyzed by XPS were essentially the same for the following two sample preparation methods: (a) dissolution of ITZ in acetone (i.e., final medium was an organic solvent) (41.92%$\pm$0.69%: 47.75%$\pm$0.59%: 10.33%$\pm$0.18%) and (b) generation of pure ITZ nanosuspension using MIVM (i.e., final medium was a water-rich medium) (42.38 $\pm$ 0.90%: 47.26%$\pm$0.73%: 10.36%$\pm$0.17%) prior to air-drying. Since these ratios were also in agreement with the theoretical value (42.11%: 47.37%: 10.53%), it could be inferred that ITZ itself did not have any orientation preference. The equations used to calculate the theoretical and experimental atomic concentration ratios of N_{ITZ}:$C_{(286\text{-}288),ITZ}$:$C_{(288\text{-}290),ITZ}$ are provided in Appendix A.1.1 and A.1.2, respectively.

The hydrophilic parts of TPGS and PEG-PLA are both PEG. Since PEG does not contribute to $C_{(288\text{-}290)}$ signal, $C_{(288\text{-}290),L,AS}$ can serve as a tracer for the hydrophobic part of pure TPGS or PEG-PLA. Using the experimental data, the relative atomic concentration of $C_{(286\text{-}288),H,AS}$ can be directly computed by subtracting the portion borne by $C_{(286\text{-}288),L,AS}$ from the relative atomic concentration of $C_{(286\text{-}288)}$ on the assumption that $C_{(286\text{-}288),L,AS}$ and $C_{(288\text{-}290),L,AS}$ are synchronously detected (Assumption 1 in Appendix A.2.2). Based on this assumption, the minimum value of $C_{(286\text{-}288),H,AS}$ was calculated and used as a tracer for the hydrophilic part of TPGS or PEG-PLA. Calculations of the theoretical and experimental relative atomic concentrations of $C_{(288\text{-}290),L,AS}$ and $C_{(286\text{-}288),H,AS}$ in pure TPGS or PEG-PLA are presented in Appendix A.2.1 and A.2.2 respectively.

For each ITZ-AS nanoparticle system, since ITZ itself has been shown to have no orientation preference, the experimental atomic concentration ratio of N_{ITZ}:$C_{(286\text{-}288),ITZ}$:$C_{(288\text{-}290),ITZ}$ can be assumed to be the same on the surface of pure ITZ particle and ITZ-AS nanoparticles (Assumption 2 in Appendix A.3.2). In other

words, the experimental relative atomic concentration of $C_{(286\text{-}288),ITZ}$ and $C_{(288\text{-}290),ITZ}$ on the surface of ITZ-AS nanoparticles can be determined based on the detected relative atomic concentration of N. By subtracting the experimental relative atomic concentration of $C_{(286\text{-}288),ITZ}$ and $C_{(288\text{-}290),ITZ}$ from that of $C_{(286\text{-}288)}$ and $C_{(288\text{-}290)}$, the experimental relative atomic concentration of $C_{(286\text{-}288),H,AS}$ and $C_{(288\text{-}290),L,AS}$ was obtained (see Appendix A.3.2). Calculation of the theoretical atomic concentration ratio of $C_{(288\text{-}290),ITZ}$:$C_{(286\text{-}288),H,AS}$:$C_{(288\text{-}290),L,AS}$ is shown in Appendix A.3.1.

The relative ratio of hydrophilic to hydrophobic part of stabilizers ($R_{H:L}$) is the atomic concentration ratio of $C_{(286\text{-}288),H,AS}$: $C_{(288\text{-}290),L,AS}$ and the data are presented in Fig. 8. Fig. 9 shows the relative ratio of ITZ to the total hydrophilic and hydrophobic parts of the stabilizer ($R_{D:H+L}$), that is, the atomic concentration ratio of $C_{(288\text{-}290),ITZ}$ to [$C_{(286\text{-}288),H,AS}$ + $C_{(288\text{-}290),L,AS}$]. Atomic concentration ratio of $C_{(286\text{-}288),H,AS}$ to [$C_{(288\text{-}290),ITZ}$ + $C_{(288\text{-}290),L,AS}$] depicts the relative ratio of hydrophilic part of the stabilizer to ITZ plus hydrophobic part of the stabilizer ($R_{H:D+L}$) on nanoparticle surface (Fig. 10).

The theoretical $R_{H:L}$ was calculated for the case of homogenously distributed hydrophilic and hydrophobic segments of stabilizers on the surface of the nanoparticles in the presence and absence of ITZ. The theoretical values and numerical results for $R_{H:L}$, $R_{D:H+L}$ and $R_{H:D+L}$ of stabilizers on the surface of the nanoparticles with or without ITZ are tabulated in Table 2.

In general, the $R_{H:L}$ values of all the nanoparticle samples obtained right after production were found to be different from the theoretical estimates, indicative of preferred orientation of the stabilizers during particle formation. From the perspective of thermodynamics, the orientation of ASs attains their equilibrium state when their hydrophobic segments form the hydrophobic core and their hydrophilic segments protrude into the surrounding water to form a micellar structure. In this circumstance, $R_{H:L}$ would tend towards infinity. Nevertheless, the determined $R_{H:L}$ values of the freshly prepared products were finite, suggesting that the stabilizers were far from the equilibrium state. In other words, the products were not in a micellar form even though the concentrations of stabilizers were above their CMCs (Table 1) and the PEG surface coverage on nanoparticles was poor or incomplete. Zhu also reached a

similar conclusion by comparing the experimental and calculated micellar particle sizes and PIs of different AS-stabilized beta-carotene nanoparticles (Zhu, 2013).

For freshly prepared blank nanoparticles of TPGS and PEG-PLA 2k-2k, the observed $R_{H:L}$ values were less than their theoretical estimates whereas the reverse was true for the PEG-PLA 2k-10k and PEG-PLA 5k-10k blank samples. This is perhaps not surprising, since with the same type of hydrophobic block (PLA), a longer hydrophobic block in PEG-PLAs (2k-10k and 5k-10k) would induce a stronger hydrophobic force for self-assembly, and thus result in more of the hydrophobic block being directed towards the particle core. When ITZ was present in the nanosystems, the $R_{H:L}$ with PEG-PLA increased but that with TPGS decreased. Since ASs are capable of regulating the growth of ITZ nuclei, they should be able to interact with ITZ at the molecular level, leading to a change in $R_{H:L}$ compared with blank nanosystems without ITZ. TPGS comprises of PEG and vitamin E succinate, and the data in Table 1 show that the solubility parameter difference ($|\Delta\delta_{ITZ}|$) between PEG and ITZ is smaller than that between vitamin E succinate and ITZ, implying higher miscibility and hence higher affinity strength between PEG and ITZ. In other words, PEG has a higher tendency to attach to ITZ than does vitamin E succinate. This tendency may outweigh the hydrophobic force exhibited by the relatively short hydrophobic block, leading to a relatively small $R_{H:L}$. For the PEG-PLAs, PEG and PLA have similar $|\Delta\delta_{ITZ}|$. When the block length of PLA is longer than that of PEG, PLA has relatively high hydrophobicity and thus stronger binding to ITZ, resulting in a relatively high $R_{H:L}$. This has been substantiated by the observation that the $R_{H:L}$ of PEG-PLA 2k-10k was the highest among the all PEG-PLAs tested (2k-2k, 2k-10k, and 5k-10k), consistent with its relatively short block length of PEG and long block length of PLA. It is worth noting that ASs probably have little time to interact with water during extremely rapid nanoprecipitation. Consequently, the affinity between PEG and water does not appear critical for nanoparticle formation.

For all freshly prepared nanoparticle formulations, the values of all $R_{D:H+L}$ were not equal or close to zero, suggesting that the drug was not fully shielded by the stabilizers. The theoretical $R_{D:H+L}$ followed in ascending order of TPGS < PEG-PLA 2k-2k < PEG-PLA 5k-10k < PEG-PLA 2k-10k. However, the experimental $R_{D:H+L}$

were closely similar ($p > 0.05$), implying that the degree of adsorption of ASs on particle surface may extensively depend on the nature of hydrophobic drug core. If the surface composition of nanoparticles remained essentially unchanged with time, $R_{H:D+L}$ would correlate well with particle stability, i.e., larger $R_{H:D+L}$ would reflect more stable nanoparticles. However, while the most stable ITZ-TPGS nanoparticles showed the lowest $R_{H:D+L}$, the $R_{H:D+L}$ of the least stable ITZ-PEG-PLA 2k-10k was larger than those of ITZ-TPGS and ITZ-PEG-PLA 5k-10k but similar to that of ITZ-PEG-PLA 2k-2k. The lack of correlation between $R_{H:D+L}$ and particle stability for freshly prepared samples would imply the occurrence of molecular rearrangement of ITZ and/or ASs during storage. This deduction was confirmed by subsequent analysis of the surface composition of nanoparticles after storage for 2 h, which revealed substantial changes in $R_{H:L}$, $R_{D:H+L}$ and $R_{H:D+L}$ ($p < 0.05$).

For all freshly prepared blank AS nanosystems, the associated $R_{H:L}$ increased after storage ($p < 0.05$), implying that AS molecules orientated towards their most stable equilibrium state during storage. Blank nanosystem composed of TPGS or PEG-PLA 2k-2k displayed a larger increase in $R_{H:L}$ compared with PEG-PLA 2k-10k and PEG-PLA 5k-10k, suggesting that the former two ASs displayed faster molecular movement and re-orientation of their hydrophilic groups towards the external aqueous phase. As TPGS is water-soluble but the tested PEG-PLAs are not (as attested by detection of particles present using DLS analysis for pure PEG-PLAs, but not for pure TPGS in water), TPGS molecules can move freely in the medium and re-orientate quickly towards the most stable arrangement at sufficiently high concentrations (i.e., above the CMC) while the mobilities of different MW PEG-PLAs are limited. Table 1 shows that the measured glass transition temperatures of the various PEG-PLAs decrease in descending order of 2k-10k > 5k-10k > 2k-2k, and the molecular mobilities of these polymers are expected to follow the reverse rank order (Lee et al., 2014).

Among all the AS-protected ITZ nanoparticle formulations, only the formulation with PEG-PLA 2k-10k maintained a similar $R_{H:L}$ during storage ($p > 0.05$). It is quite likely that the strong hydrophobic attraction between ITZ and the PLA moiety of PEG-PLA, coupled with the inherently low mobility of PEG-PLA

2k-10k, have rendered molecular re-orientation of PEG-PLA towards the most stable micelle-like structure extremely slow. The PEG-PLA in the drug nanoparticles was found to show no significant molecular rearrangement and desorption. Interestingly, the formulation with PEG-PLA 2k-10k showed an increase in $R_{D:H+L}$ after storage ($p < 0.05$) despite having an essentially unchanged $R_{H:L}$. In view of the fact that this nanoparticle preparation yielded negligible amount of free drug in the suspending medium, the increase in drug proportion at the particle surface was likely to be due to an outward diffusion of solubilized ITZ from the core to the particle surface. Such solubilization or mobilization of ITZ in the core may be induced by its close association with the relatively mobile PLA block of the stabilizer. Once the mobilized ITZ reached the external aqueous medium, it would precipitate again to form relatively coarse particles.

The situations were apparently more complicated for the formulations containing TPGS, PEG-PLA 2k-2k and PEG-PLA 5k-10k because the three stabilizers displayed significant movement during storage, as suggested by significant changes in their $R_{H:L}$ during storage ($p < 0.05$) (Fig. 8). It is likely that TPGS, having the highest mobility, adsorbed rapidly on the "outward bound" ITZ, resulting in a lower drug content on the particle surface, as reflected by a decrease in $R_{D:H+L}$ after storage ($p < 0.05$) (Fig. 9). Meanwhile, the hydrophilic PEG groups in TPGS were being drawn towards the external aqueous medium. TPGS continued to undergo molecular rearrangement towards its thermodynamic equilibrium state while confining ITZ to the particle core, as suggested by an increase in $R_{H:L}$ after storage ($p < 0.05$) (Fig. 8). On the other hand, the molecular movement of both PEG-PLA 2k-2k and PEG-PLA 5k-10k was probably lower than that of ITZ so that a larger proportion of ITZ not being adsorbed by the stabilizer could diffuse outwards to the particle surface after storage, as indicated by an increase in $R_{D:H+L}$ ($p < 0.05$). The stability problem appeared to be more critical with PEG-PLA 5k-10k than with PEG-PLA 2k-2k, since the former nanoparticle system displayed an even lower $R_{H:L}$ after storage, implying an even higher propensity of the hydrophilic PEG groups to re-orientate towards the hydrophobic particle core and the lipophilic groups to move towards the hydrophilic particle surface. Such an increase in severity of the anomalous reorientation of the

stabilizer molecules may be explained by the concomitant outward migration of a larger amount of solubilized ITZ molecules from the particle core, which carry along with them a certain portion of the physically attached hydrophobic tails of the stabilizer towards the particle surface. As mentioned earlier, such drug-induced anomalous molecular re-orientation of the stabilizer is dependent on the molecular mobility and drug solubilizing capacity of the stabilizer. Based on its T_g (Table 1), PEG-PLA 2k-10k should have the lowest molecular mobility among the three PEG-PLAs tested, and in terms of solubilizing capacity, it should be comparable to PEG-PLA 5k-10k, which has an equivalent-sized PLA segment (Rekatas et al., 2001). Unlike PEG-PLAs 2k-2k and 5k-10k, PEG-PLA 2k-10k displayed an essentially unchanged $R_{H:L}$ after storage, suggesting that the outward migration of solubilized ITZ exerts no impact on the re-orientation of the stabilizer molecules. The lack of such impact may be explained by an exceptionally low molecular mobility of PEG-PLA 2k-10k. In fact, the order of stability of ITZ-AS nanoparticles was found to follow the order of mobility of ASs used but not the order of $R_{H:L}$ or $R_{H:D+L}$ of nanoparticles (Fig. 8 and 10). The rapid rearrangement of ASs during storage can greatly help to reduce particle aggregation and drug leakage from nanoparticles. Fig. 11 summarizes the re-orientation and rearrangement process of ASs with various mobilities in ITZ nanoparticles.

3.5. Morphology and phase imaging of ITZ-AS nanoparticles

Tapping-mode AFM (TM-AFM) allows observation of heterogeneous materials with enhanced contrast through phase imaging. Fig. 12 shows the topographic and phase image of ITZ-TPGS nanoparticles before and after storage. The nanoparticles were roughly spherical in shape, and the observed size was in agreement with the results obtained by DLS particle sizing. It has been reported that the PEG blocks have a lower stiffness than the PLA blocks in the PEG-PLA co-block polymers, and hence can be differentiated from the latter by their darkened image (Essa et al., 2010). For the ITZ-TPGS nanoparticles in the present study, this technique is expected to reveal a black coating on the nanoparticles if the PEG blocks in TPGS are sufficiently concentrated on the surface of the nanoparticles and directed

towards water. Fig. 12 shows an absence of a clearly darkened region on the ITZ-TPGS nanoparticles, suggesting that the surface of the nanoparticles was not completely covered by the PEG groups prior to and after storage even though the molecular rearrangement of TPGS might have proceeded for quite some time. This inference for incomplete PEG surface coverage accorded well with that based on the XPS study where the $R_{H:L}$ value was still finite initially, but approached infinity after storage (see Section 3.4). Fig. 12b shows the presence of relatively small lumps on the surface of a huge particle, indicative of particle aggregation and an apparent increase in particle size during storage.

4. Conclusions

TPGS-stabilized ITZ nanoparticles with initial particle size less than 100 nm and PI below 0.2 have been successfully generated by FNP using a four-stream MIVM. The short-term stability of the nanoparticle formulation is significantly better than the other reported cases of storage stability for particular ITZ nanoparticle formulations in the literature. Elucidation of the actual packing structure of ASs in nanoparticles is critical for devising effective strategies for circumventing the stability problem. Ideally, to achieve maximum stability for the nanoparticles, ASs should assume the most stable molecular orientation or arrangement in the nanoparticles with their hydrophobic tails adsorbed on nucleating drug particles and hydrophilic heads directing towards the external aqueous medium (i.e., a micelle-like structure). It was found that ASs were not in this most stable structure in both freshly prepared blank and drug-loaded nanosystems. This is mainly attributable to the highly efficient mixing of antisolvent and solution streams, and consequential extremely rapid precipitation (within milliseconds) of the nanoparticles in the MIVM. Since the nanoparticles are formed within such a short time-scale, the AS therein does not have sufficient time to undergo re-orientation and rearrangement to the most stable equilibrium state. Differences in the interaction strength between the hydrophobic segment of AS and drug as well as between the hydrophilic segment of AS and drug were seen to govern the orientation of AS during particle formation. In the absence of drug, ASs in blank nanosystems can more readily re-orientate towards their

thermodynamic equilibrium position. Since solubilized ITZ inside the hydrophobic particle core can diffuse to and precipitate on particle surface, ASs need to move faster than ITZ in order to maintain adequate protection for ITZ from the surrounding aqueous medium and to continue the molecular rearrangement process until completion. Mobility of ASs was found to exert a greater influence on the stability of drug-loaded nanoparticles than the initial packing structure of ASs in the nanoparticles. XPS has been shown to be an invaluable tool for monitoring the time-dependent change in surface structure of rapidly formed nanoparticles. The present findings may have important implications for the selection of effective amphiphilic stabilizers for the formulation of stable drug nanoparticles.

Acknowledgement

Financial supports from The Chinese University of Hong Kong (Postgraduate Studentship for KYW) and The University of Hong Kong (Faculty Start-up Fund for SFC; 204600519) are gratefully acknowledged. The authors also thank Prof. Robert K. Prud'homme (Department of Chemical and Biological Engineering, Princeton University) for assistance with refabrication of an MIVM at CUHK.

Figures and Tables

Stabilizer/drug	**Concentration of stabilizer in nanosuspensions (μM)**	**CMC at room temperature (μM)**	**T_g (℃)**	**δ_{ITZ} or $\delta_{stabilizer}$ $((MJ/m^3)^{1/2})^b$**	**$\lvert\Delta\delta_{PEG}\rvert$ $((MJ/m^3)^{1/2})$**	**$\lvert\Delta\delta_{ITZ}\rvert$ $((MJ/m^3)^{1/2})$**
ITZ	---	---	59 (Six et al., 2001)	26.5 (Bellantone et al., 2012)	5.1	0
PEG	---	---	---	~21.4 (Zhu, 2013)	0	5.1
Vitamin E succinate	---	---	---	19.0[b]	2.4	7.5
PLA	---	---	---	~21.3 (Zhu, 2013)	0.1	5.2
TPGS	163.4	20 (Sadoqi et al., 2009)	---	---	---	---
PEG-PLA 2k-2k	62.5	4.5 (Garofalo et al., 2013)	-42.72[a]	---	---	---
PEG-PLA 2k-10k	20.8	< 0.95, CMC decreases with increasing the MW of	13.85[a]	---	---	---

		PLA (Yang et al., 2007)			
PEG-PLA 5k-10k	16.7	< 3.8 (Garofalo et al., 2013)	-16.61[a]	---	---	---

[a] Determined by DSC

[b] Calculated using the method of Hoy (Barton, 1991)

Table 1. Properties of ITZ and stabilizers ($\Delta\boldsymbol{\delta}_{\boldsymbol{PEG}} = \boldsymbol{\delta}_{\boldsymbol{ITZ/stabilizer}} - \boldsymbol{\delta}_{\boldsymbol{PEG}}$; $\Delta\boldsymbol{\delta}_{\boldsymbol{ITZ}} = \boldsymbol{\delta}_{\boldsymbol{stabilizer}} - \boldsymbol{\delta}_{\boldsymbol{ITZ}}$)

Nanosystems containing solely stabilizer (without ITZ)		$R_{H:L}$		
TPGS	Theoretical value	23		
	Right after preparation	10.194 ± 0.334		
	After storage for 2 h	14.909 ± 0.945		
PEG-PLA 2k-2k	Theoretical value	3.214		
	Right after preparation	2.553 ± 0.299		
	After storage for 2 h	5.628 ± 0.741		
PEG-PLA 2k-10k	Theoretical value	0.647		
	Right after preparation	1.692 ± 0.119		
	After storage for 2 h	2.186 ± 0.057		
PEG-PLA 5k-10k	Theoretical value	1.640		
	Right after preparation	2.177 ± 0.121		
	After storage for 2 h	2.668 ± 0.107		
ITZ nanoparticles with stabilizer		**$R_{H:L}$**	**$R_{D:H+L}$**	**$R_{H:D+L}$**
ITZ nanoparticles with TPGS	Theoretical value	23	0.09	7.255
	Right after preparation	0.933 ± 0.049	0.104 ± 0.003	0.777 ± 0.038
	After storage for 2 h	12.241 ± 0.786	0.031 ± 0.001	8.680 ± 0.401
ITZ nanoparticles with PEG-PLA 2k-2k	Theoretical value	3.214	0.096	2.287
	Right after preparation	10.531 ± 0.408	0.100 ± 0.003	4.883 ± 0.111
	After storage for 2 h	7.281 ± 0.313	0.141 ± 0.004	3.359 ± 0.131
ITZ nanoparticles with PEG-PLA 2k-10k	Theoretical value	0.647	0.149	0.520
	Right after preparation	10.63 ± 0.217	0.104 ± 0.002	4.822 ± 0.110
	After storage for 2 h	10.694 ± 0.144	0.144 ± 0.006	3.981 ± 0.121
ITZ nanoparticles with PEG-PLA 5k-10k	Theoretical value	1.640	0.116	1.256
	Right after preparation	7.939 ± 0.399	0.104 ± 0.004	4.113 ± 0.138
	After storage for 2 h	3.722 ± 0.332	0.162 ± 0.008	2.107 ± 0.156

Table 2. Result summary from the XPS study (n=3)

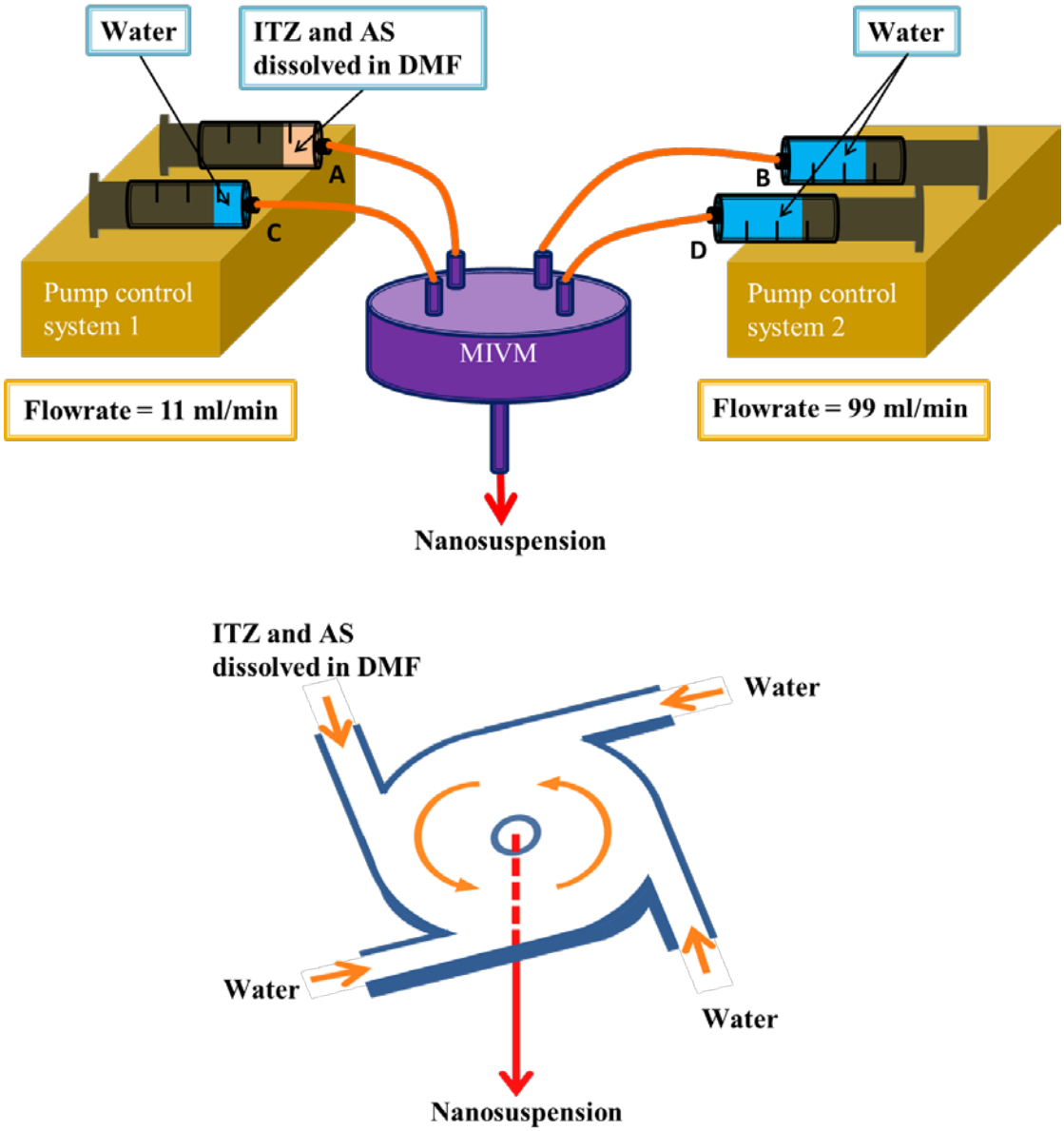

Fig. 1. Preparation of drug nanosuspensions using MIVM.

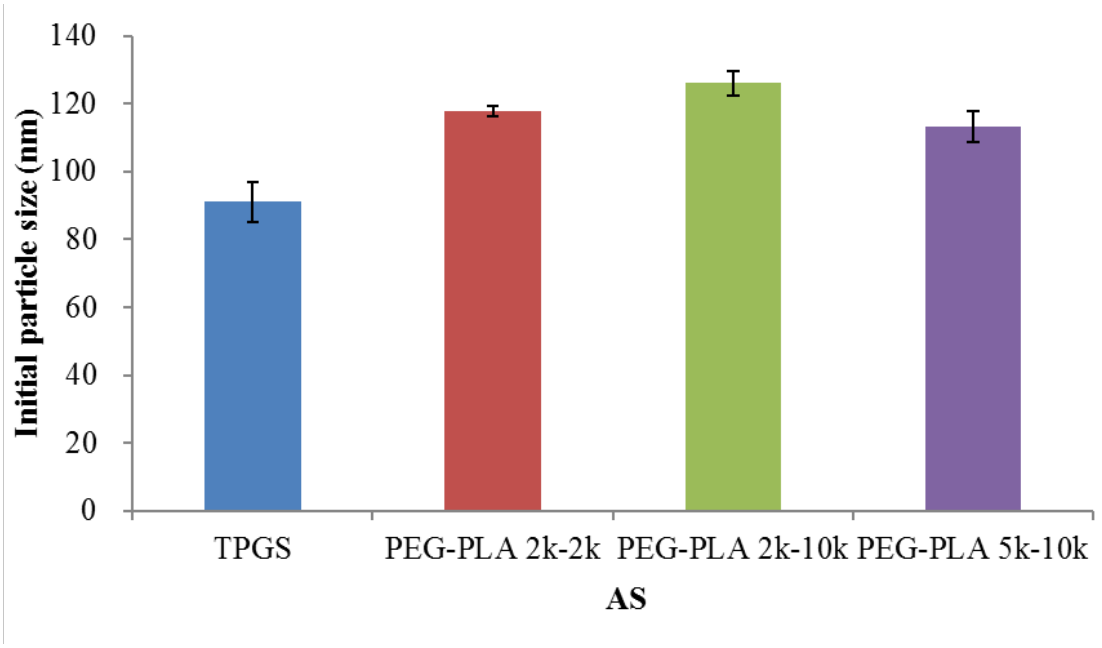

Fig. 2. Initial particle size of ITZ nanoparticles prepared with various stabilizers (ITZ:stabilizer = 1:1 w/w; n = 3).

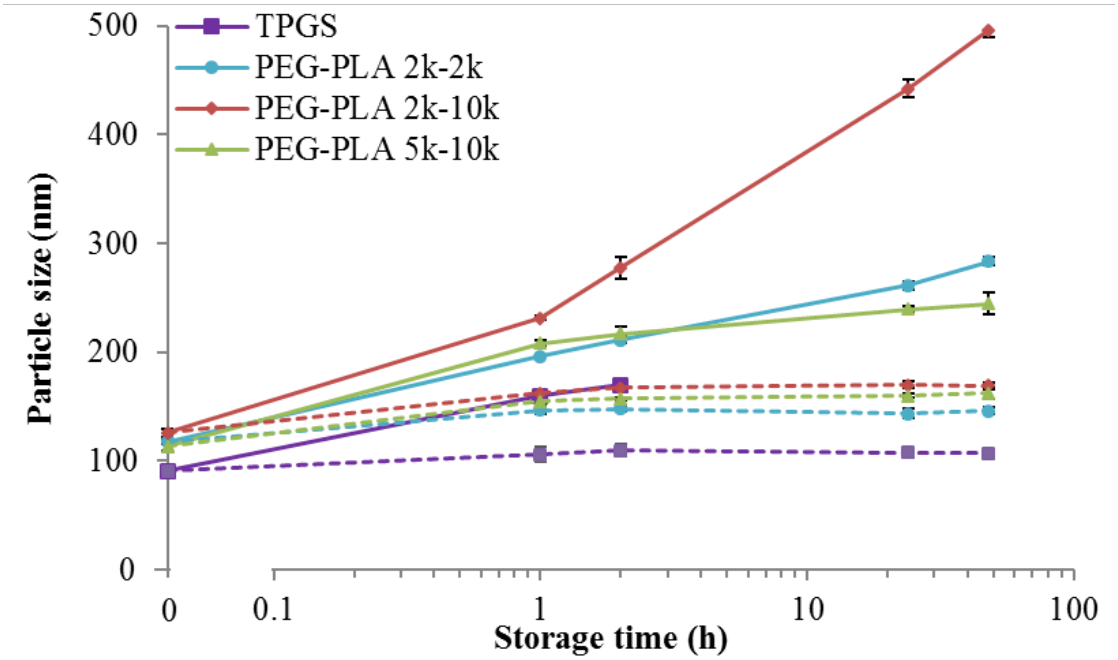

Fig. 3. Stability profiles of ITZ nanosuspensions with TPGS and PEG-PLA. Solid lines and dotted lines represent the nanosuspensions stored at room temperature and refrigerated condition, respectively (n = 3).

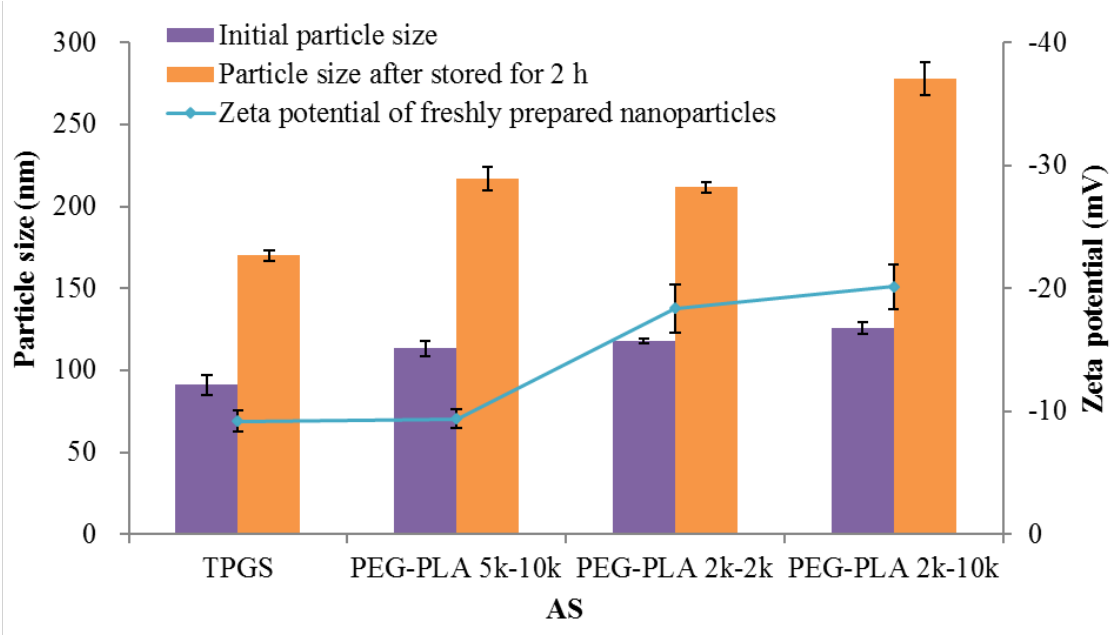

Fig. 4. Correlation of zeta potential, initial particle size and stability of ITZ-AS nanoparticles (n = 3).

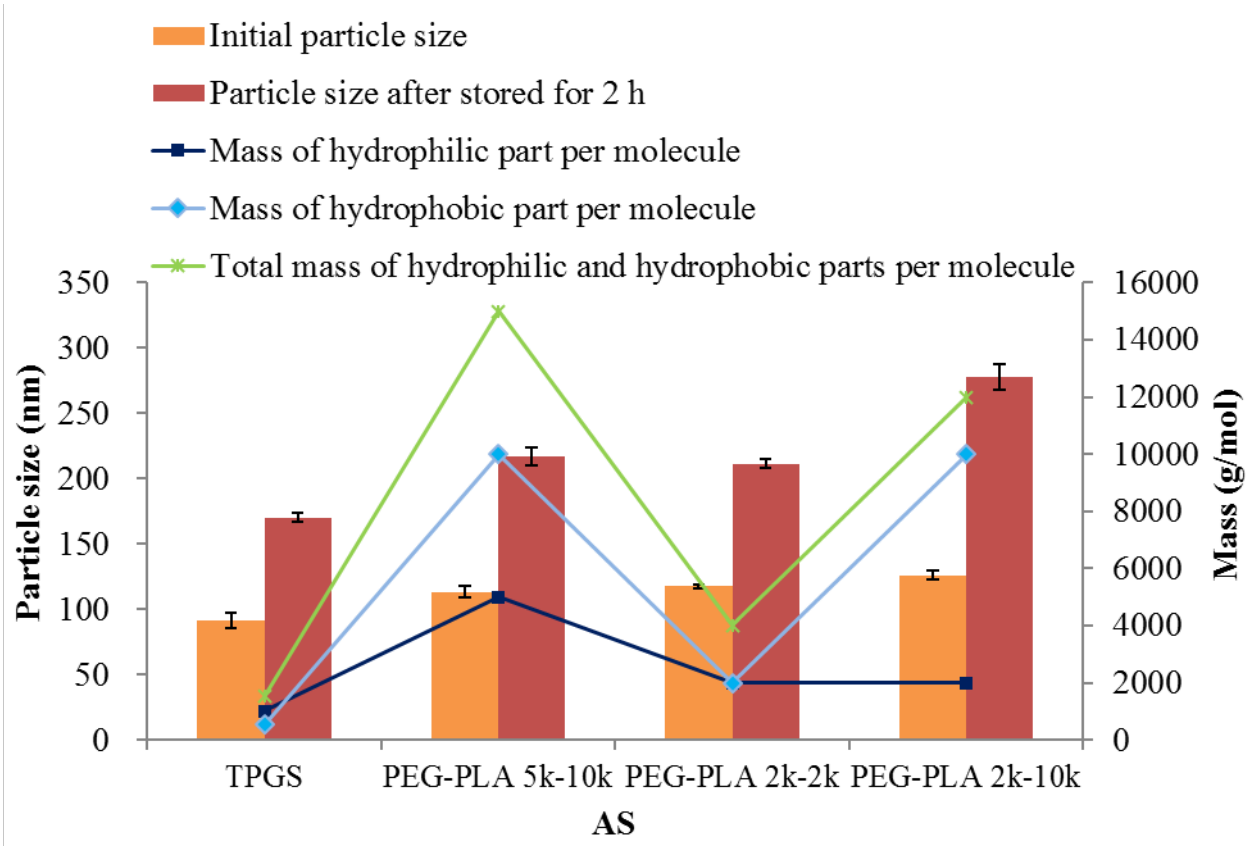

Fig. 5. Correlation of MW, initial particle size (n = 3) and stability (n = 3) of ITZ-AS nanoparticles.

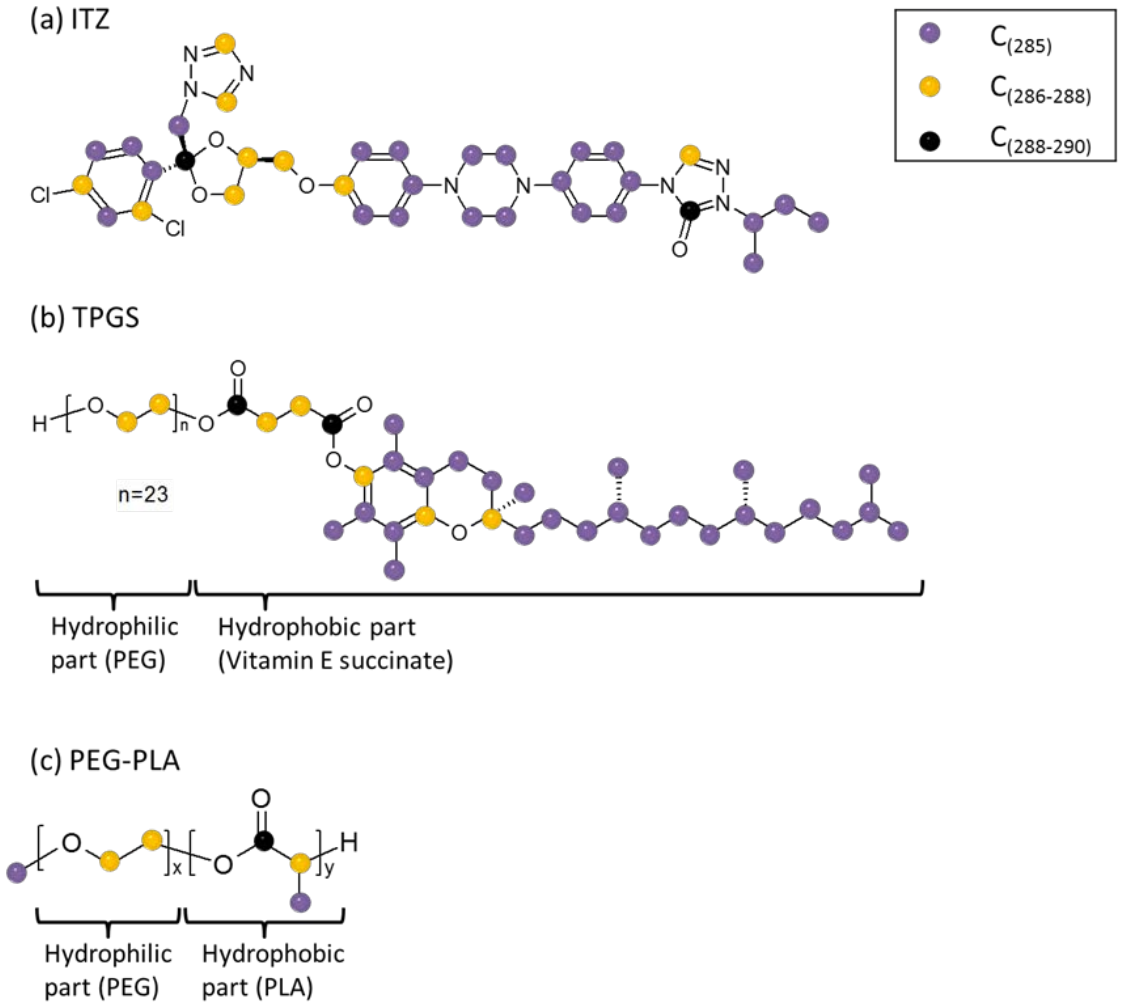

Fig. 6. Classification of carbon binding energy ranges in ITZ, TPGS and PEG-PLA.

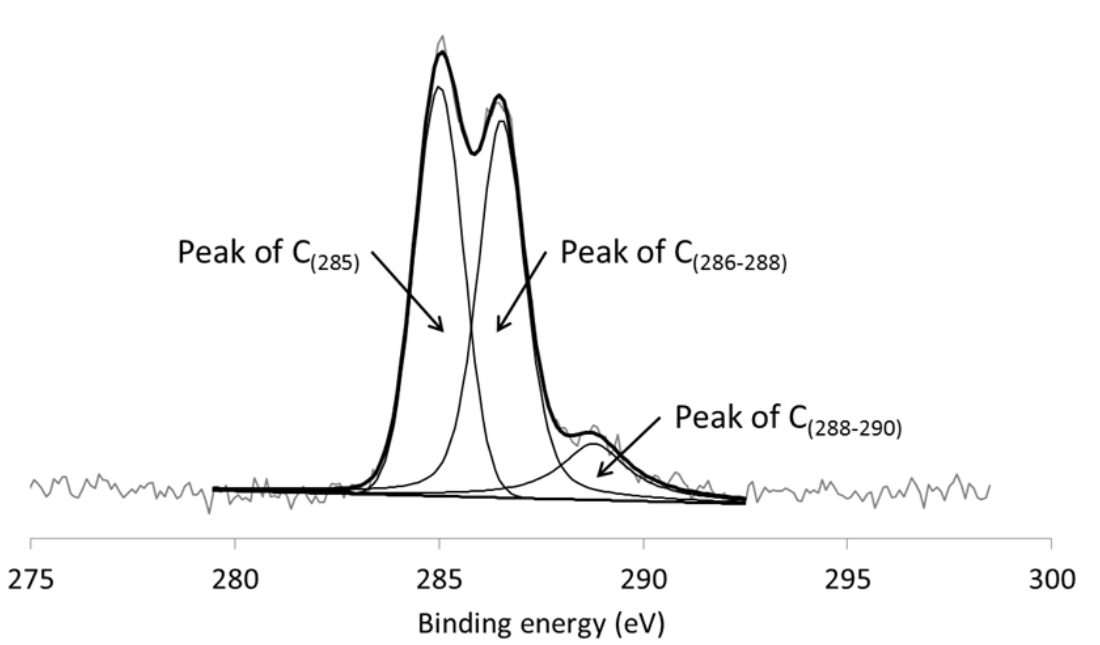

Fig. 7. Representative XPS peak fitting of freshly prepared ITZ-TPGS nanoparticles (ITZ:TPGS = 1:1 w/w).

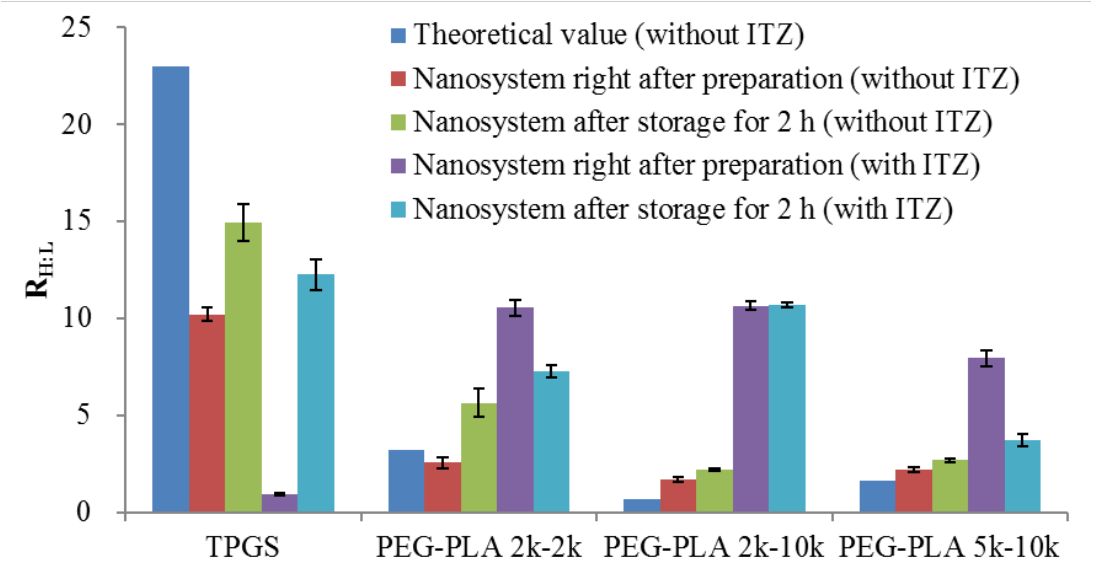

Fig. 8. Atomic concentration ratio of $C_{(286\text{-}288),H,AS}$ to $C_{(288\text{-}290),L,AS}$ ($R_{H:L}$; n=3).

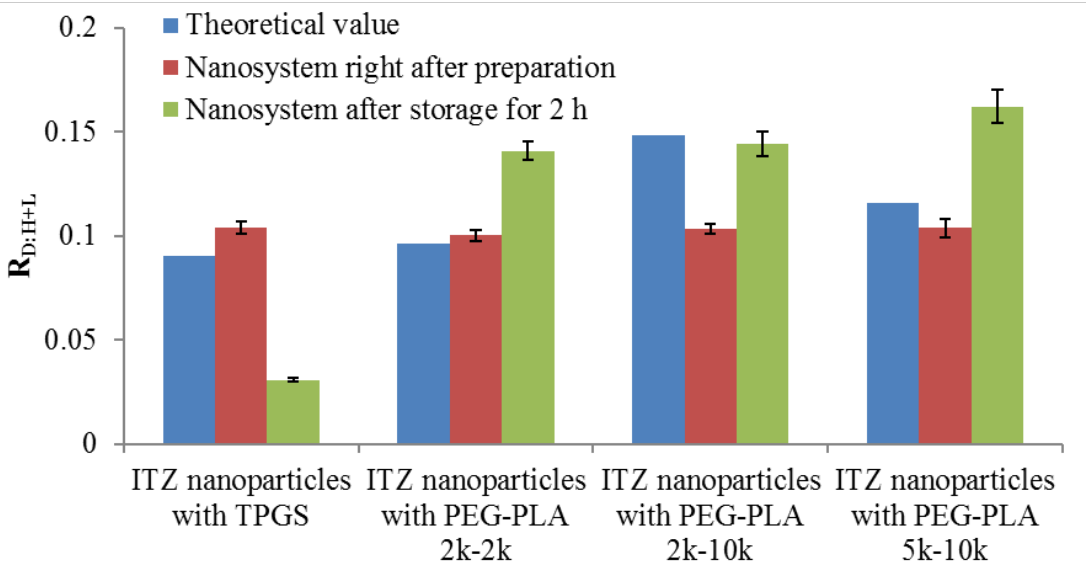

Fig. 9. Atomic concentration ratio of $C_{(288-290),ITZ}$ to $[C_{(286-288),H,AS} + C_{(288-290),L,AS}]$ ($R_{D:H+L}$; n=3).

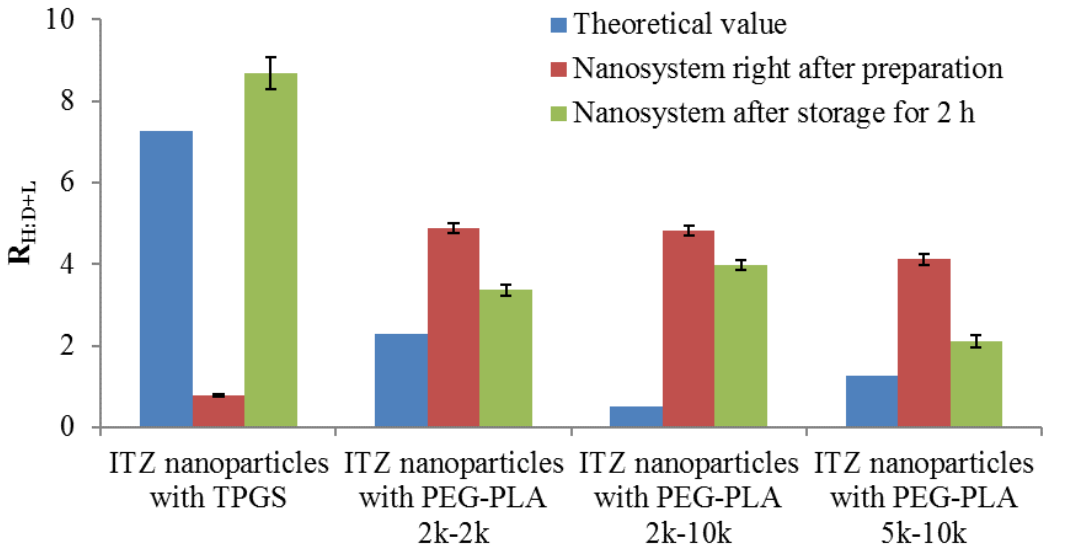

Fig. 10. Atomic concentration ratio of $C_{(286-288),H,AS}$ to $[C_{(288-290),ITZ} + C_{(288-290),L,AS}]$ ($R_{H:D+L}$; n=3).

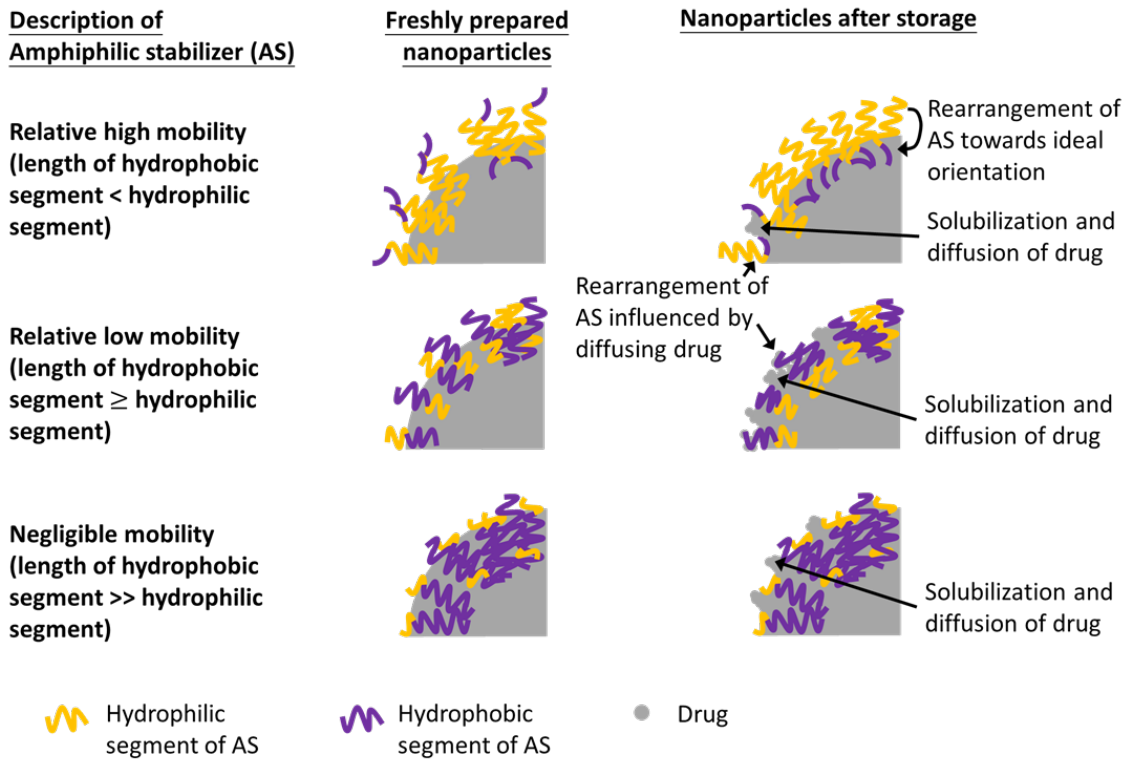

Fig. 11. A schematic diagram illustrating structural packing of AS in ITZ nanoparticles right after production and after 2 h of storage.

(a)

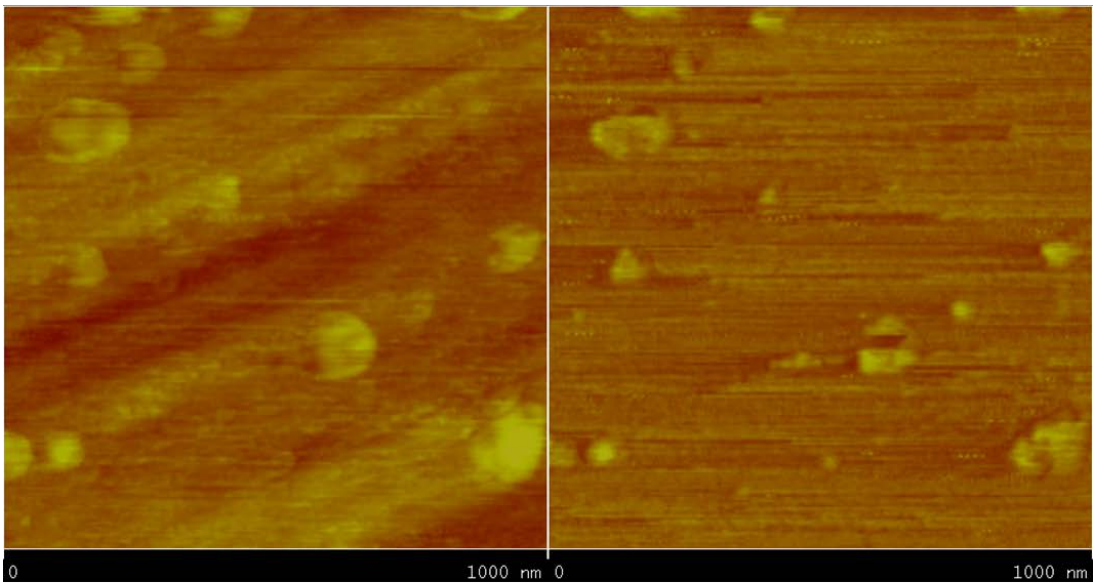
0
1000 nm
0
1000 nm

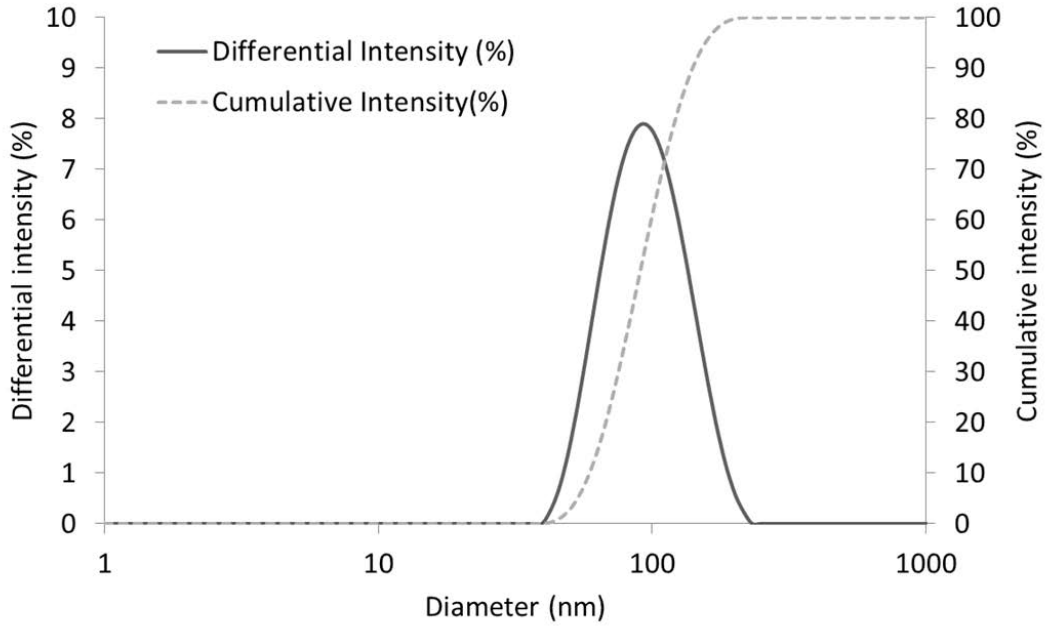
Differential Intensity (%)
Cumulative Intensity(%)
Differential intensity (%)
Cumulative intensity (%)
Diameter (nm)
0
1
2
3
4
5
6
7
8
9
10
0
10
20
30
40
50
60
70
80
90
100
1
10
100
1000

(b)

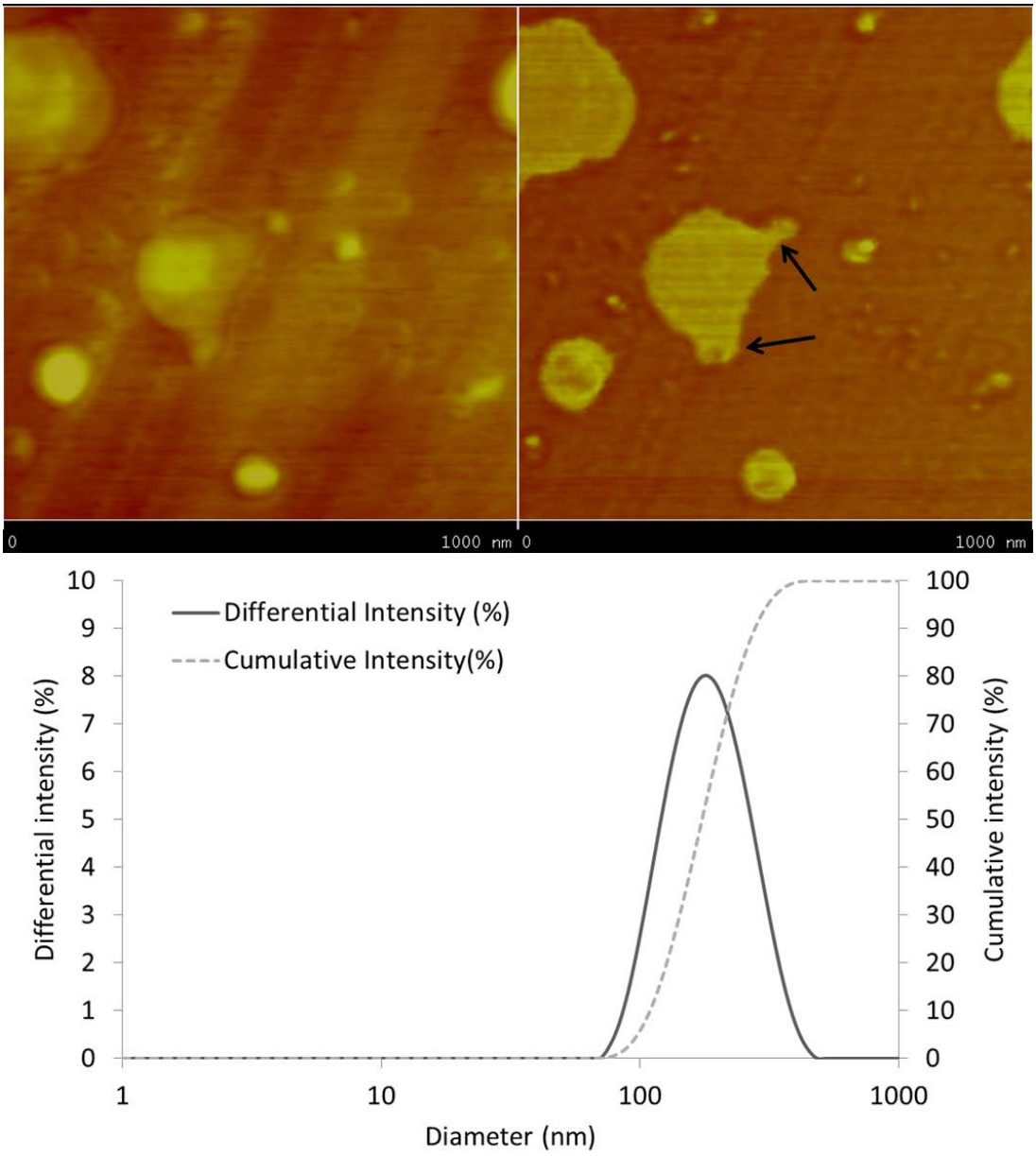

Fig. 12. Topographic image (top left), phase image (top right) and particle size distribution (bottom) of ITZ-TPGS nanoparticles (a) right after production and (b) after storage of 2 h (small lumps on a huge particle were indicated by arrows).

References

Ahmed, F., Discher, D.E., 2004. Self-porating polymersomes of PEG-PLA and PEG-PCL: hydrolysis-triggered controlled release vesicles. J Control Release 96, 37-53.

Allen, T.M., Cullis, P.R., 2004. Drug delivery systems: entering the mainstream. Science 303, 1818-1822.

Barton, A.F., 1991. CRC handbook of solubility parameters and other cohesion parameters. CRC press.

Bascom, W., Chen, W., 1991. Effect of plasma treatment on the adhesion of carbon fibers to thermoplastic polymers. The Journal of Adhesion 34, 99-119.

Bellantone, R.A., Patel, P., Sandhu, H., Choi, D.S., Singhal, D., Chokshi, H., Malick, A.W., Shah, N., 2012. A method to predict the equilibrium solubility of drugs in solid polymers near room temperature using thermal analysis. J Pharm Sci 101, 4549-4558.

Briggs, D., 1977. Handbook of X-Ray and Ultraviolet Photoelectron Spectroscopy, Heyden & Son Ltd. London, UK.

Chan, H.-K., Kwok, P.C.L., 2011. Production methods for nanodrug particles using the bottom-up approach. Advanced drug delivery reviews 63, 406-416.

Chen, W., Gu, B., Wang, H., Pan, J., Lu, W., Hou, H., 2008. Development and evaluation of novel itraconazole-loaded intravenous nanoparticles. Int J Pharm 362, 133-140.

Cholkar, K., Hariharan, S., Gunda, S., Mitra, A.K., 2014. Optimization of dexamethasone mixed nanomicellar formulation. AAPS PharmSciTech 15, 1454-1467.

Chow, S.F., Sun, C.C., Chow, A.H.L., 2014. Assessment of the relative performance of a confined impinging jets mixer and a multi-inlet vortex mixer for curcumin nanoparticle production. European Journal of Pharmaceutics and Biopharmaceutics 88, 462-471.

Chow, S.F., Wan, K.Y., Cheng, K.K., Wong, K.W., Sun, C.C., Baum, L., Chow, A.H.L., 2015. Development of highly stabilized curcumin nanoparticles by flash nanoprecipitation and lyophilization. European Journal of Pharmaceutics and Biopharmaceutics 94, 436-449.

Collnot, E.M., Baldes, C., Wempe, M.F., Hyatt, J., Navarro, L., Edgar, K.J., Schaefer, U.F., Lehr, C.M., 2006. Influence of vitamin E TPGS poly(ethylene glycol) chain length on apical efflux transporters in Caco-2 cell monolayers. J Control Release 111, 35-40.

Collnot, E.M., Baldes, C., Wempe, M.F., Kappl, R., Huttermann, J., Hyatt, J.A., Edgar, K.J., Schaefer, U.F., Lehr, C.M., 2007. Mechanism of inhibition of P-glycoprotein mediated efflux by vitamin E TPGS: influence on ATPase activity and membrane

fluidity. Mol Pharm 4, 465-474.
Essa, S., Rabanel, J.M., Hildgen, P., 2010. Effect of polyethylene glycol (PEG) chain organization on the physicochemical properties of poly(D, L-lactide) (PLA) based nanoparticles. Eur J Pharm Biopharm 75, 96-106.
Fernandes, C., Soni, U., Patravale, V., 2010. Nano-interventions for neurodegenerative disorders. Pharmacol Res 62, 166-178.
Garofalo, C., Capuano, G., Sottile, R., Tallerico, R., Adami, R., Reverchon, E., Carbone, E., Izzo, L., Pappalardo, D., 2013. Different insight into amphiphilic PEG-PLA copolymers: influence of macromolecular architecture on the micelle formation and cellular uptake. Biomacromolecules 15, 403-415.
Italia, J.L., Bhatt, D.K., Bhardwaj, V., Tikoo, K., Kumar, M.N., 2007. PLGA nanoparticles for oral delivery of cyclosporine: nephrotoxicity and pharmacokinetic studies in comparison to Sandimmune Neoral. J Control Release 119, 197-206.
Jacobs, C., Kayser, O., Müller, R., 2000. Nanosuspensions as a new approach for the formulation for the poorly soluble drug tarazepide. International journal of pharmaceutics 196, 161-164.
Johnson, B.K., Prud'homme, R.K., 2003. Flash nanoprecipitation of organic actives and block copolymers using a confined impinging jets mixer. Australian Journal of Chemistry 56, 1021-1024.
Jung, J.-Y., Yoo, S.D., Lee, S.-H., Kim, K.-H., Yoon, D.-S., Lee, K.-H., 1999. Enhanced solubility and dissolution rate of itraconazole by a solid dispersion technique. International journal of pharmaceutics 187, 209-218.
Kim, J.K., Park, J.S., Kim, C.K., 2010. Development of a binary lipid nanoparticles formulation of itraconazole for parenteral administration and controlled release. Int J Pharm 383, 209-215.
Kumar, V., Wang, L., Riebe, M., Tung, H.-H., Prud’homme, R.K., 2009. Formulation and stability of itraconazole and odanacatib nanoparticles: governing physical parameters. Molecular pharmaceutics 6, 1118-1124.
Lee, T.W., Boersen, N.A., Hui, H.W., Chow, S.F., Wan, K.Y., Chow, A.H., 2014. Delivery of poorly soluble compounds by amorphous solid dispersions. Curr Pharm Des 20, 303-324.
Liu, Y., Cheng, C.Y., Liu, Y., Prud'homme, R.K., Fox, R.O., 2008a. Mixing in a multi-inlet vortex mixer (MIVM) for flash nano-precipitation. Chem Eng Sci 63, 2829-2842.
Liu, Y., Kathan, K., Saad, W., Prud'homme, R.K., 2007. Ostwald ripening of beta-carotene nanoparticles. Phys Rev Lett 98, 036102.
Liu, Y., Tong, Z., Prud'homme, R.K., 2008b. Stabilized polymeric nanoparticles for controlled and efficient release of bifenthrin. Pest Manag Sci 64, 808-812.

Miyama, T., Takanaga, H., Matsuo, H., Yamano, K., Yamamoto, K., Iga, T., Naito, M., Tsuruo, T., Ishizuka, H., Kawahara, Y., Sawada, Y., 1998. P-glycoprotein-mediated transport of itraconazole across the blood-brain barrier. Antimicrob Agents Chemother 42, 1738-1744.

Nasongkla, N., Bey, E., Ren, J., Ai, H., Khemtong, C., Guthi, J.S., Chin, S.-F., Sherry, A.D., Boothman, D.A., Gao, J., 2006. Multifunctional polymeric micelles as cancer-targeted, MRI-ultrasensitive drug delivery systems. Nano letters 6, 2427-2430.

Pustulka, K.M., Wohl, A.R., Lee, H.S., Michel, A.R., Han, J., Hoye, T.R., McCormick, A.V., Panyam, J., Macosko, C.W., 2013. Flash nanoprecipitation: particle structure and stability. Mol Pharm 10, 4367-4377.

Rabinow, B., Kipp, J., Papadopoulos, P., Wong, J., Glosson, J., Gass, J., Sun, C.S., Wielgos, T., White, R., Cook, C., Barker, K., Wood, K., 2007. Itraconazole IV nanosuspension enhances efficacy through altered pharmacokinetics in the rat. Int J Pharm 339, 251-260.

Rekatas, C.J., Mai, S.-M., Crothers, M., Quinn, M., Collett, J.H., Attwood, D., Heatley, F., Martini, L., Booth, C., 2001. The effect of hydrophobe chemical structure and chain length on the solubilization of griseofulvin in aqueous micellar solutions of block copoly (oxyalkylene) s. Physical Chemistry Chemical Physics 3, 4769-4773.

Riley, T., Stolnik, S., Heald, C., Xiong, C., Garnett, M., Illum, L., Davis, S., Purkiss, S., Barlow, R., Gellert, P., 2001. Physicochemical evaluation of nanoparticles assembled from Poly (lactic acid)− Poly (ethylene glycol)(PLA− PEG) block copolymers as drug delivery vehicles. Langmuir 17, 3168-3174.

Russ, B., Liu, Y., Prud'homme, R.K., 2010. Optimized descriptive model for micromixing in a vortex mixer. Chemical Engineering Communications 197, 1068-1075.

Saad, W.S., 2007. Drug nanoparticle formation via flash nanoprecipitation: conjugation to encapsulate and control the release of paclitaxel. Ph.D. Dissertation, Princeton University, Princeton.

Sadoqi, M., Lau-Cam, C.A., Wu, S.H., 2009. Investigation of the micellar properties of the tocopheryl polyethylene glycol succinate surfactants TPGS 400 and TPGS 1000 by steady state fluorometry. J Colloid Interface Sci 333, 585-589.

Six, K., Verreck, G., Peeters, J., Binnemans, K., Berghmans, H., Augustijns, P., Kinget, R., Van den Mooter, G., 2001. Investigation of thermal properties of glassy itraconazole: identification of a monotropic mesophase. Thermochimica acta 376, 175-181.

Van Peer, A., Woestenborghs, R., Heykants, J., Gasparini, R., Gauwenbergh, G., 1989. The effects of food and dose on the oral systemic availability of itraconazole in healthy subjects. European journal of clinical pharmacology 36, 423-426.

Yang, L., Zhao, Z., Wei, J., El Ghzaoui, A., Li, S., 2007. Micelles formed by self-assembling of polylactide/poly(ethylene glycol) block copolymers in aqueous solutions. J Colloid Interface Sci 314, 470-477.
Zhang, Y.Y., Feng, J., McManus, S.A., Lu, H.D., Ristroph, K.D., Cho, E.J., Dobrijevic, E.L., Chan, H.K., Prud'homme, R.K., 2017. Design and Solidification of Fast-Releasing Clofazimine Nanoparticles for Treatment of Cryptosporidiosis. Molecular Pharmaceutics 14, 3480-3488.
Zhu, Z., 2013. Effects of amphiphilic diblock copolymer on drug nanoparticle formation and stability. Biomaterials 34, 10238-10248.
Zhu, Z., 2014. Flash nanoprecipitation: prediction and enhancement of particle stability via drug structure. Mol Pharm 11, 776-786.
Zhu, Z., Anacker, J.L., Ji, S., Hoye, T.R., Macosko, C.W., Prud'homme, R.K., 2007. Formation of block copolymer-protected nanoparticles via reactive impingement mixing. Langmuir 23, 10499-10504.
Zhu, Z., Margulis-Goshen, K., Magdassi, S., Talmon, Y., Macosko, C.W., 2010. Polyelectrolyte stabilized drug nanoparticles via flash nanoprecipitation: A model study with β-carotene. Journal of pharmaceutical sciences 99, 4295-4306.